
# Frequency-Based Virtual-Admittance Tuning for Grid-Forming Converters

# Frequency-Based Virtual-Admittance Tuning for Grid-Forming Converters

Paul Imgart*, Mebtu Beza*, Massimo Bongiorno*, Jan R. Svensson† and Jean-Philippe Hasler‡
* Department of Electrical Engineering
Chalmers University of Technology
Göteborg, Sweden
paul.imgart@chalmers.se
† Hitachi Energy Research
Västerås
Sweden
‡ Hitachi Energy
Västerås
Sweden

***Abstract*—Grid-forming (GFM) converter control is a key technology enabling stable operation of converter-dominated electric power grids, which makes the converter behave as a slowly varying voltage source behind an impedance. The utilization of a virtual admittance (VA) in the converter control allows to choose this impedance at frequencies above the active range of the power controllers. Moreover, employing a decoupled GFM controller allows to choose the VA parameters freely without introducing power coupling. This paper proposes a VA parameter tuning approach that bases the parameter selection on the desired frequency response of the controller, either specified as gain limits for the input admittance at two chosen frequencies, or as a decay time constant for the VA's synchronous frequency resonance. Finally, the impact of the parameter choice on the converter's response to grid disturbances is investigated.**

***Index Terms*—Frequency response, grid-forming control, grid-forming inverters, virtual impedance.**

## I. Introduction

The amount of electricity generation from renewable sources is increasing to limit climate change through the reduction of greenhouse gas emissions [1]. Alongside other factors such as increased utilization and flexibility assets in the power system as well as changing consumer technologies, this results in an increasing share of power electronics in electric power grids [2]. This increase gives rise to concerns regarding the stability of converter-dominated power grids. Examples for the challenges related to this are the decrease of mechanical inertia, reduced short-circuit current and risk of adverse control interaction [3].

Grid-forming (GFM) converter control, in which the converter is controlled to act as a slowly varying voltage source behind an impedance, is discussed widely as a solution for these challenges [3], [4]. As a consequence of this behaviour, the converter's behaviour at other frequencies than the fundamental as well as its dynamic response to disturbances are mainly determined by the impedance in this representation. Among the GFM control variants in the literature, the virtual admittance (VA) based control is a popular approach, which allows to tune this behaviour by choosing the VA parameters appropriately [5]–[7].

Submitted to the 24th Power Systems Computation Conference (PSCC 2026).

Classical implementations of the VA-based control require a predominantly inductive VA to ensure decoupling between active power and angle of the controller's internal voltage on one hand, and reactive power and the magnitude of the internal voltage on the other hand [5]. On the other hand, the decoupled GFM control presented in [8] is a modification of the classical implementation which employs a VA phase compensation to allow free selection of the VA parameters without introducing coupling between active and reactive power in the active frequency range of the power controllers (PCs). As a consequence, both virtual resistance and inductance provide a degree of freedom each in tuning the controller.

For frequencies that, in the synchronous reference frame (SRF), lie between the closed-loop bandwidth of the PCs and of an eventual current controller (CC), the VA parameters dictate the behaviour of the converter. This can be illustrated with the help of the understanding that the GFM converter should behave as a slowly varying voltage source behind an impedance [8], [9]: At frequencies above the active range of the PCs and the synchronous-frequency resonance (SFR), the converter ideally appears as an impedance to the grid, and in the decoupled controller this impedance corresponds to the virtual impedance, $\underline{Y}_\mathrm{v}^{-1}$. For typical bandwidths, this range is from around $50\,\mathrm{Hz}$ up to the loop bandwidth of eventual inner loops [8]. In consequence, the VA largely defines the converter's behaviour, in particular during transients and in the harmonic range.

There is a large number of tuning approaches for VAs in GFM control structures available in the existing literature. Depending on the intended purpose of the VA in the control structure in question, the proposed tuning approaches vary greatly:

- *Power sharing:* A large group of publications (e.g. [10]–[16]) employs an adaptive VA to ensure (typically reactive or harmonic) power sharing. This methods are typically developed for a microgrid context, and use the VA as a droop. The majority of VA-based GFM control structures, including the decoupled controller studied here, use PCs that control the active power at the converter terminals or the point of common coupling (PCC), thereby eliminating any droop effect from the VA. Furthermore, the aforementioned tuning methods tune the VA parameters at specific

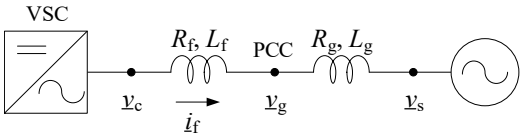


Fig. 1: Single-line circuit diagram of the investigated system.

frequencies, in most cases the fundamental, disregarding the impact at the rest of the frequency spectrum.

- *Current limitation:* Another common tuning approach is for using the virtual impedance (VI) to limit the converter current [17]–[21]. This approach does not offer any support in selecting the VA in the linear operating range of the converter.
- *Stability analysis:* Other publications study through eigenvalue analysis the impact of the VA parameters on the converter's stability [18], [22]–[30]. Ensuring stability is extremely important, but these analysis methods offer little support in choosing the parameters within the stable region.
- *Current reference generation and filtering:* In this group of publications the VA fills a comparable function in the investigated control structure as in the decoupled controller. They typically suggest a value of $0.3\,\mathrm{pu}$ to $0.5\,\mathrm{pu}$ for the virtual inductance, motivating this by the similarity to typical synchronous machine (SM) transient reactances [5], [7], [31]. $R_\mathrm{v}$ is consequently selected based on the desired time constant of the VA (between the outer and inner control loop's bandwidth). These approaches take the VA's impact on the converter's frequency response at most indirectly into account.
- *Impact on frequency response:* Only very few publications discuss VA parameter tuning with this aim. Reference [32] considers how a low-pass filtered $\underline{Y}_\mathrm{v}^{-1}$ can improve stability and damping in a microgrid. The presented tuning approach requires knowledge of the complete system to conduct an eigenvalue analysis, which is often impossible to acquire in real applications, and is difficult to generalise. In [33], the impact of virtual inductance and resistance on stability and damping is discussed in relative terms, but no tuning procedure is suggested to motivate the parameter selection for the simulations in the paper.

These tuning approaches are either irrelevant or offer little support in terms of actual tuning method when the goal is to utilize the VA parameters to shape the converter's frequency response during normal operation, and not primarily during transients. A tuning approach that fully considers the impact of the VA parameters on the desired GFM converter behaviour is therefore required.

Based on these findings, this paper provides a VA parameter tuning method to shape the converter's frequency response. It is organised as follows: Section II contains a description of the desired GFM frequency response. This is followed by a description of the proposed VA parameter tuning method in Section III. In Section IV, the tuning criteria are related to the dominant resonance decay constant and Section V to the converter's transient response to disturbance. The paper's conclusions are given in Section VI. The source code for a software implementation of the tuning method proposed in this work is available at [34].

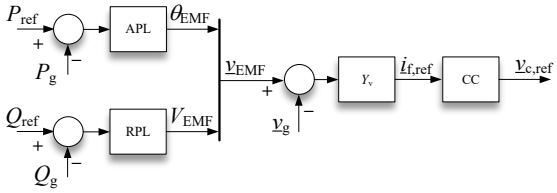


Fig. 2: Generalised structure of VA-GFM control strategy.

## II. Desired GFM Frequency Response

To illustrate the proposed tuning method, a simple system consisting of a voltage source converter (VSC), an L-filter (represented by $L_\mathrm{f}$ and $R_\mathrm{f}$) and a grid represented by its Thévenin equivalent consisting of $L_\mathrm{g}$, $R_\mathrm{g}$ and $\underline{v}_\mathrm{s}$ is investigated as illustrated in Fig. 1. The VSC's terminal voltage is denoted as $v_\mathrm{c}$, the terminal current into the filter as $i_\mathrm{f}$ and the PCC voltage is $v_\mathrm{g}$. The desired frequency response of a GFM converter can be analysed using the generalised GFM control with a VA as shown in Fig. 2. In this diagram, $P_\mathrm{ref}$ and $Q_\mathrm{ref}$ denote the active- and reactive-power reference, $P_\mathrm{g}$ and $Q_\mathrm{g}$ the active and reactive power injected into the grid at the PCC, $V_\mathrm{EMF}$ and $\theta_\mathrm{EMF}$ the converter's (virtual) internal voltage's magnitude and angle, respectively, and APL and RPL are the active- and reactive power loop, respectively.

The desired response can be understood recalling that GFM behaviour means the converter acts as a slowly varying voltage source behind an impedance. It is important to stress that the slow variation of the internal voltage is what allows the converter to control active- and reactive power transfer. This is not specific for converter-based generation, but applies to SMs as well. In consequence, the converter shows constant-power behaviour up to the speed of its outer (power) control loops. Such constant-power behaviour results in an input admittance which in the SRF decreases asymptotically towards a fixed, setpoint-dependent negative resistance as the frequency decreases[1] [35].

At higher frequencies, i.e. in the harmonic range, the converter should act as an impedance with inductive or inductive-resistive behaviour, which corresponds to a decreasing input admittance [3]. In this way, the converter provides passive damping by acting as a sink for harmonic currents, which improves voltage quality and grid strength at the PCC. Constant inductive-resistive impedance[2] behaviour also means that the converter is passive and does not contribute to adverse control interactions within the controllable frequency range [3]. This constant-impedance behaviour extends up to the end of the active range of the controller's inner control loops, e.g. CC or

[1]To avoid confusion, this paper will solely use SRF where not explicitly stated differently.

[2]Constant impedance refers in this work to fixed resistance and inductance, i.e. a frequency-dependent impedance.

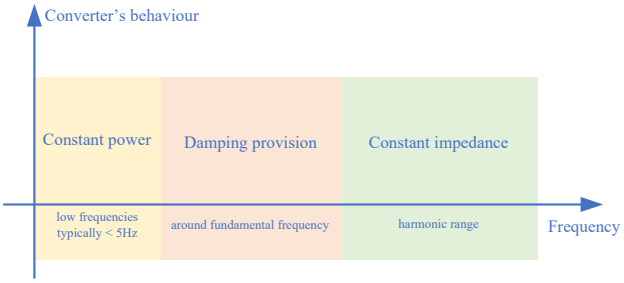


Fig. 3: Desired GFM control behaviour at different frequencies.

modulation stage, as beyond this point the VA-representation deteriorates.

In the transition between the active range of the power loops and the harmonic range, the converter should provide damping to reduce the impact of the SFR and to contribute to power oscillation damping, as due to the SRF's frequency shift subsynchronous phenomena are located in this range [36], [37]. Combining these requirements together, the desired GFM frequency response – serving as a guideline for control-parameter tuning – is shown in Fig. 3. The following section shows how the proposed VA tuning method allows to select the VA parameters based on the desired frequency response in the "damping provision" and "constant impedance" areas.

## III. Proposed Tuning Method

For the proposed tuning method, the desired converter frequency response is defined based on the definition of upper limits for the gain of the converter's input admittance at two selected frequencies. As shown below, these requirements are then used to determine the VA parameters. The next section then demonstrates how the gain limit can be replaced by transient performance requirements such as a decay time constant.

The proposed tuning method is illustrated using the decoupled VA-GFM control introduced in [8], as this GFM control allows free selection of the virtual resistance without introducing undesired power coupling between the active-power loop (APL) and reactive-power loop (RPL) in the frequency region where these controllers are active. However, the tuning method proposed here is applicable independent of the chosen type of VA-GFM control, as the previously described desired frequency behaviour is common among them. As shown in [8], the impact of the decoupled controller's outer loops on the converter's input admittance can for zero power setpoints be modelled by multiplication with a second order high-pass filter of the form $s^2/(s+\alpha)^2$, where $\alpha$ is the bandwidth of the respective outer loop. This representation assumes that the outer loops' damping ratio is equal to one. For power setpoints differing from zero, the input admittance will not approach zero for a decreasing frequency, but will instead approach a small, fixed, setpoint-dependent value, reflecting the constant power behaviour of the outer loops. As the frequency range of interest for the tuning of the VA parameters is above the power loops' bandwidth, the impact of the power setpoint can be neglected for the purposes of this paper. Under these assumptions and neglecting the impact of eventual inner control loops, the converter's input admittance is for the decoupled controller given as

$$\boldsymbol{Y}_\mathrm{c} = \begin{bmatrix} \underline{Y}_\mathrm{dd} & \underline{Y}_\mathrm{dq} \\ \underline{Y}_\mathrm{qd} & \underline{Y}_\mathrm{qq} \end{bmatrix} = \begin{bmatrix} \frac{R_\mathrm{v}+sL_\mathrm{v}}{A}\frac{s^2}{(s+\alpha_\mathrm{P})^2} & \frac{\omega_\mathrm{c}L_\mathrm{v}}{A}\frac{s^2}{(s+\alpha_\mathrm{P})^2} \\ \frac{-\omega_\mathrm{c}L_\mathrm{v}}{A}\frac{s^2}{(s+\alpha_\mathrm{Q})^2} & \frac{R_\mathrm{v}+sL_\mathrm{v}}{A}\frac{s^2}{(s+\alpha_\mathrm{Q})^2} \end{bmatrix}, \quad \text{where} \quad A = (R_\mathrm{v}+sL_\mathrm{v})^2 + (\omega_\mathrm{c}L_\mathrm{v})^2. \tag{1}$$

$R_\mathrm{v}$ and $L_\mathrm{v}$ are the virtual resistance and inductance, $\alpha_\mathrm{P}$ and $\alpha_\mathrm{Q}$ are the APL's and RPL's bandwidths, respectively, and $\omega_\mathrm{c}$ is the angular frequency of the converter's internal voltage source. For the tuning process, $\omega_\mathrm{c} \approx \omega_\mathrm{b}$ is assumed in the input admittance since the grid frequency, and the internal voltage source's frequency accordingly, typically only show small variations. For the rest of this paper, the speed of the two power control loops is assumed to be equal: $\alpha_\mathrm{p} = \alpha_\mathrm{Q} = 5\ 2\pi\ \mathrm{rad/s}$, which results in a Hermitian input admittance:

$$\underline{Y}_\mathrm{dd} = \underline{Y}_\mathrm{qq} \qquad \text{and} \qquad \underline{Y}_\mathrm{dq} = -\underline{Y}_\mathrm{qd}. \tag{2}$$

In the proposed tuning method, an upper limit is established for the gain of the virtual admittance at two frequencies to tune the two VA parameters, $R_\mathrm{v}$ and $L_\mathrm{v}$. The first frequency should be the location of the SFR, as this is the frequency where the gain of the input admittance reaches its maximum. For higher $R/X$ ratios, this resonance becomes more damped and the natural frequency moves from $\omega_\mathrm{b}$ towards higher frequencies. The natural frequency, neglecting the impact of the outer loops, can be estimated from (1) as

$$\omega_\mathrm{n} = \sqrt{\omega_\mathrm{b}^2 + \frac{R_\mathrm{v}^2}{L_\mathrm{v}^2}}. \tag{3}$$

A Bode diagram of the input admittance for $L_\mathrm{v} = 0.5\,\mathrm{pu}$ and varying $R_\mathrm{v}$ is shown in Fig. 4, with the curve in black marking the trajectory of the gain at natural frequency. While the natural frequency increases with $R_\mathrm{v}/X_\mathrm{v}$, it can be seen that for $R_\mathrm{v}/X_\mathrm{v} > 1$, i.e. damping ratios approaching 1, the highest gain moves from the natural frequency to lower frequencies due to the disappearance of the resonant peak. Since the filtering properties of the virtual inductance typically are important, a predominantly resistive tuning of the VA is not to be expected. This means that the natural frequency remains a good choice for the location of the first gain limit. As the natural frequency depends on the chosen $R/X$ ratio, the tuning process becomes iterative.

The second frequency can be chosen more freely. Commonly, the lowest harmonics present in the grid above the fundamental negative sequence are the fifth and seventh harmonics. Since the fifth harmonic is a negative sequence, and the seventh is a positive sequence, both appear at $6\omega_\mathrm{b}$ in the SRF. This makes this frequency a sensible choice for the second gain limit, choosing a required attenuation at the lowest harmonics present in the grid.

Using (1), the input admittance's gain is computed at the two selected frequencies and shown in Figures 5 and 6. To

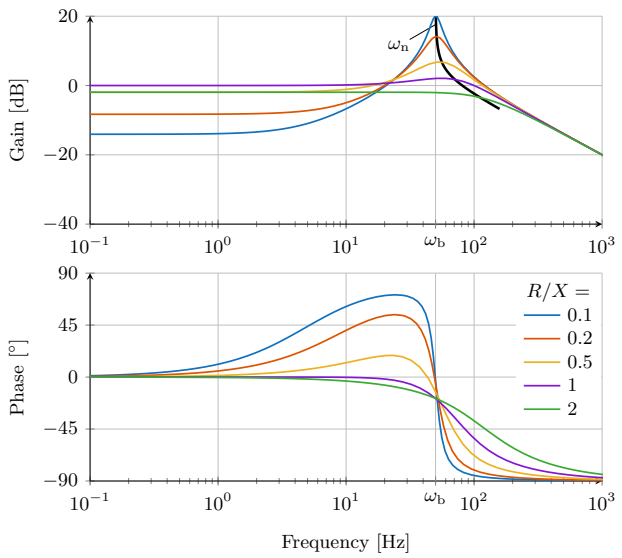


Fig. 4: Bode diagram of the diagonal elements of the input admittance for $L_v = 0.5\,\text{pu}$ and varying resistance. Impact of the outer loops is neglected. In black: trajectory of the gain at natural frequency.

maintain readability, the plots have been limited to a gain of $5\,\text{pu}$ and $1\,\text{pu}$, respectively. The figures illustrate that for most of the area of interest, the gain of the off-diagonal elements of the input-admittance matrix ($|\underline{Y}_{dq}| = |\underline{Y}_{qd}|$) is lower than the diagonal elements' gain ($|\underline{Y}_{dd} = \underline{Y}_{qq}|$), which based on the analysis of the decoupled controller's frequency response in [8] is expected. Assuming the same speed for both PCs, the off-diagonal elements only have a higher gain around the natural frequency of a very poorly damped SFR. As a parameter combination with a poorly damped SFR is not expected to be desirable, the tuning process is based on the gain of the diagonal elements. The change of the contour lines' slope between Fig. 5 and Fig. 6 demonstrates how the impact of the virtual inductor on the gain increases with the frequency: Around the natural frequency, the VA's resistive component is dominant, while the inductive component is mainly responsible for the behaviour at higher frequencies.

Consequently, the gain limits at the two selected frequencies can be formulated as

$$|\underline{Y}_{dd}(j\omega_n)| \leq m_1 \quad \text{and} \tag{4}$$

$$|\underline{Y}_{dd}(j6\omega_b)| \leq m_2, \tag{5}$$

where $m_1$ and $m_2$ are the chosen gain limits. As can be seen in Figures 5 and 6, the gain of the VA's diagonal elements is monotonously decreasing in both variables, i.e. an increase in either parameter leads to a reduced gain. As a consequence, minimum values for the parameters that observe the gain limits in (4) and (5) can be estimated by replacing the inequality with an equality. This allows to estimate an $R_v$ for each $L_v$ so that the gain limit is exactly fulfilled.

To complete the tuning process, both requirements are combined. This is illustrated in Fig. 7 for two example cases: case 1 which does not permit amplification at the fundamental and

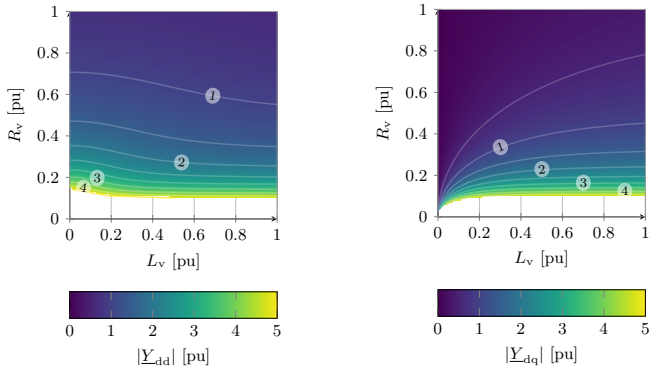


Fig. 5: Gain of the input admittance at natural frequency $\omega_n$. Specific values for $|Y_{dd}|$ and $|Y_{dq}|$ are highlighted by the contour lines.

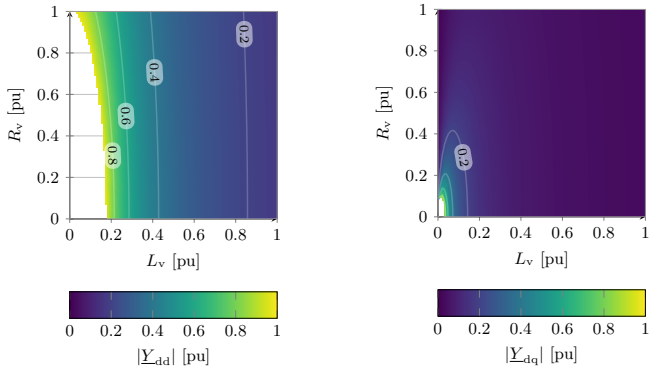


Fig. 6: Gain of the input admittance at fifth and seventh harmonic ($6\omega_b$). Specific values for $|Y_{dd}|$ and $|Y_{dq}|$ are highlighted by the contour lines.

requires strong attenuation at the fifth and seventh harmonic ($m_1 = 1\,\text{pu}$, $m_2 = 0.25\,\text{pu}$), and case 2 which permits slight amplification at the fundamental and requires less attenuation ($m_1 = 2\,\text{pu}$, $m_2 = 0.5\,\text{pu}$). At the intersection of both curves, the set of parameters exactly matches both requirements. As a consequence of the previously stated monotonously decreasing characteristic, all combinations of $R_v$ and $L_v$ above the plotted curves follow the respective requirement. The parameters corresponding to the intersection of both curves are given in Table I. Since the ratio $m_2/m_1$ is equal in case 1 and 2, the $R/X$ ratio of the resulting parameters is constant. To illustrate the consequence of a change in this ratio, a mixed case (case 3) with $m_1 = 2\,\text{pu}$ and $m_2 = 0.25\,\text{pu}$ has been defined as well, with a more dominant inductive component.

In Fig. 8, a Bode diagram of the frequency response of the resulting input admittance's diagonal elements is shown for all three cases. As the minimum parameters for cases 1 and 2 have the same $R/X$ ratio, the resulting frequency response is

TABLE I: Gain limits and resulting minimum VA parameters for example cases 1-3.

| Case | $m_1$ | $m_2$ | $L_v$ | $R_v$ | $R_v/X_v$ |
|---|---|---|---|---|---|
| Case 1 | 1 pu | 0.25 pu | 0.676 pu | 0.596 pu | 0.882 |
| Case 2 | 2 pu | 0.5 pu | 0.338 pu | 0.298 pu | 0.882 |
| Case 3 | 2 pu | 0.25 pu | 0.684 pu | 0.26 pu | 0.38 |

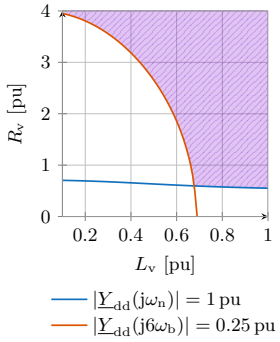


(a) Combination of the gain limits for example case 1.

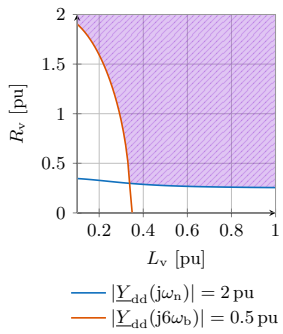


(b) Combination of the gain limits for example case 2.

Fig. 7: Graphical combination of the parameter combinations exactly respecting the gain limits. Parameters in the shaded area fulfil (4) and (5). Observe the different scaling of the $y$-axis.

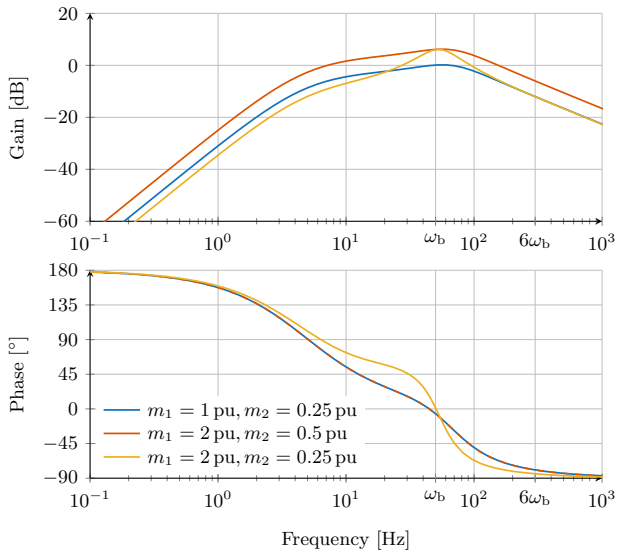


Fig. 8: Bode diagram of the diagonal elements of the input admittance for the parameter combinations in Table I. Blue: case 1. Red: case 2. Yellow: case 3.

just shifted vertically. Case 3 illustrates how a relatively large inductive component, here dictated by the larger attenuation at the high-frequency gain limit, causes a resonance at the natural frequency if the resistive component is not increased as well.

## IV. Relation to Decay Time Constant

The maximum gain limits formulated above relate the VA parameters to the resulting input admittance, but performance requirements in e.g. grid codes might be formulated differently. A common requirement can instead be that a direct current (dc) component caused by the SFR has to decay within a certain time. The amplitude of a damped oscillation decays with the decay time constant $\tau$ following

$$\hat{x}(t) = \hat{x}_0 \, \mathrm{e}^{-\frac{t}{\tau}}, \tag{6}$$

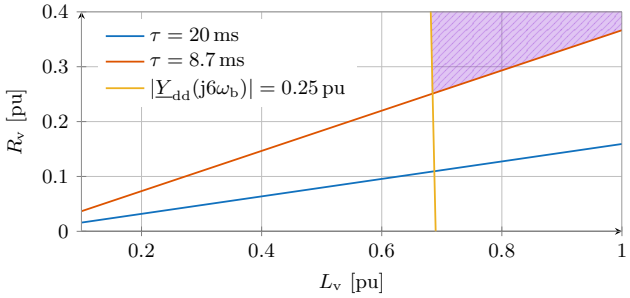


Fig. 9: Combinations of $R_v$ and $L_v$ providing the required decay time constant. The yellow curve reproduces one of the gain limits from the previous section for reference. Parameters in the shaded area result in $\tau \leq 8.7\,\mathrm{ms}$ and fulfil the reproduced gain limit.

where $t$ is the time, $\hat{x}_0$ is the amplitude of the oscillation at $t = 0$ and $\hat{x}(t)$ is the oscillation amplitude at time $t$. After time corresponding to the time constant has passed, the oscillation amplitude has reduced to $1/\mathrm{e} \approx 36.8\,\%$. If the grid code requires the oscillation to decay to a ratio of $\xi = \hat{x}(t_{\max})/\hat{x}_0$ within time $t_{\max}$, the time constant can be determined by rearranging (6) to

$$\tau = \frac{-t_{\max}}{\ln \xi}. \tag{7}$$

Neglecting the impact of the outer control loops, the damping ratio $\zeta$ is related to the time constant by $\zeta = (\omega_n \tau)^{-1}$. From (1), the damping ratio can be related to the VA parameters by

$$\zeta = \sqrt{\frac{R_v^2}{R_v^2 + \omega_b^2 L_v^2}}. \tag{8}$$

Together with (3) for $\omega_n$, this results in[3]

$$R_v = \frac{L_v}{\tau}. \tag{9}$$

Consequently, the $R/X$ ratio can be expressed as $T_b/(2\pi\tau) \approx 0.16 T_b/\tau$, with $T_b$ being one period of the fundamental frequency, i.e. 20 ms at 50 Hz. This requirement is illustrated for two cases in Fig. 9: for a time constant of $\tau = 20\,\mathrm{ms}$, and for the requirement that the dc component should decay to 10 % of its initial amplitude within one cycle, which corresponds to a time constant of $\tau = 8.7\,\mathrm{ms}$. Similar to the gain-requirement-based tuning combinations shown previously, (9) shows that all tuning combinations lying above the indicated line perform better than required, i.e. have a shorter time constant.

As shown in Fig. 9, the tuning combinations complying with the time-constant requirement have different characteristics than the gain limits due to their fixed $R/X$ ratio. While the gain limits call for a minimum value of the virtual impedance $Z_v = Y_v^{-1} = \sqrt{R_v^2 + \omega_b^2 L_v^2}$, the time constant is only depending on the $R/X$ ratio. Consequently, a larger virtual inductance requires a larger virtual resistance to keep the time constant unchanged. To illustrate this, the tuning combination

[3]It is important to note that all quantities in this equation need to either be in SI units or per-unit. The conversion for the time constant is $[\tau]_{\mathrm{pu}} = \omega_b [\tau]_{\mathrm{s}}$.

that fulfils the lower of the previously studied gain limits in the harmonic range, $|\underline{Y}_{\mathrm{dd}}(\mathrm{j}6\omega_{\mathrm{b}})| = 0.25\,\mathrm{pu}$, is shown in yellow in Fig. 9.

Similar to before, a pair of requirements is needed to tune the VA parameters. To achieve this, the time constant-based tuning according to (9) can be combined with a single gain limit, for example the one shown in yellow in Fig. 9. To illustrate the resulting frequency response, three example cases are studied: case 4, requiring a decay of the dc component to $10\,\%$ within one cycle paired with a strong attenuation for the harmonics ($\tau = 8.7\,\mathrm{ms}, m_2 = 0.25\,\mathrm{pu}$), case 5 with the same time constant but a relaxed attenuation requirement ($\tau = 8.7\,\mathrm{ms}, m_2 = 0.5\,\mathrm{pu}$), and case 6 with a larger time constant but strong attenuation ($\tau = 20\,\mathrm{ms}, m_2 = 0.25\,\mathrm{pu}$). The parameters resulting in these minimum requirements are shown in Table II, and a Bode diagram of the resulting input admittances is given in Fig. 10. A verification of the decay time constant estimation is demonstrated in [8].

While the decay time constant remains the same for case 4 and 5, simulations with the parameters in Table III reveal that the maximum amplitude of the dc component is nearly twice as high in case 5. Even though the relative reduction happens with the same speed, in terms of absolute value of the dc component the lower gain limit makes case 4 perform notably better. To give an example, the reduction of the dc component to $0.1\,\mathrm{pu}$ takes approximately $16\,\mathrm{ms}$ in case 4, while it takes $24\,\mathrm{ms}$ in case 5. This difference is due to the different size of the VI, caused by the distinct gain limits. A smaller VI results in larger currents in response to a given disturbance, and corresponds to a higher gain at the SFR's natural frequency. This is also illustrated by Fig. 10, where the frequency response's corresponding to case 4 (in blue) and 5 (in red) have the same shape, but case 5 is shifted upwards as it has a higher gain. Case 6 with the large time constant has a different $R/X$ ratio than the other two cases, which is reflected by the much more pronounced resonant peak in the resulting frequency response (in yellow). The peak value of the dc component is slightly larger than in case 4 (which shares the same gain limit $m_2$), but it takes $37\,\mathrm{ms}$ for the dc component to decay to $0.1\,\mathrm{pu}$ due to the larger time constant.

TABLE II: Time constant and gain limits and resulting minimum VA parameters for example cases 4-6.

| Case | $\tau$ | $m_2$ | $L_{\mathrm{v}}$ | $R_{\mathrm{v}}$ | $R_{\mathrm{v}}/X_{\mathrm{v}}$ |
|---|---|---|---|---|---|
| Case 4 | 8.7 ms | 0.25 pu | 0.685 pu | 0.251 pu | 0.37 |
| Case 5 | 8.7 ms | 0.5 pu | 0.345 pu | 0.126 pu | 0.37 |
| Case 6 | 20 ms | 0.25 pu | 0.687 pu | 0.109 pu | 0.16 |

TABLE III: System and control parameters for the simulation.

| System parameters | | Control parameters | |
|---|---|---|---|
| $S_{\mathrm{N}}$ | 100 MVA | $L_{\mathrm{v1}}$ | 0.343 pu |
| $V_{\mathrm{N}}$ | 400 kV | $R_{\mathrm{v1}}$ | 0.9843 pu |
| $\omega_{\mathrm{b}}$ | 314.16 rad/s | $\alpha_{\mathrm{P}} = \alpha_{\mathrm{Q}}$ | $2\pi$ 5 rad/s |
| $L_{\mathrm{f}}$ | 0.157 pu | $\zeta_{\mathrm{P}} = \zeta_{\mathrm{Q}}$ | 1 |
| $R_{\mathrm{f}}$ | 0.0157 pu | $\alpha_{\mathrm{CC}}$ | $2\pi$ 200 rad/s |
| SCR | 6.6 | | |
| $C_{\mathrm{sh}}$ | 0.0942 pu | | |

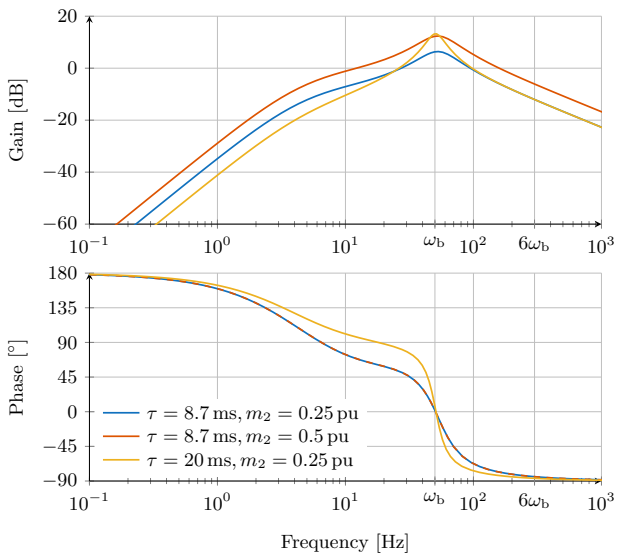


Fig. 10: Bode diagram of the diagonal elements of the input admittance for the parameter combinations in Table II. Blue: case 4. Red: case 5. Yellow: case 6.

These observations show that the time constant can be a meaningful addition to the previously presented gain limits, but it needs to be paired with a single gain limit to confine the dc component in absolute terms.

## V. VA-Parameter Impact on Transient Disturbance Response

As the preceding analysis has established that the gain of the input admittance is monotonously decreasing for increasing $R_{\mathrm{v}}$ and $L_{\mathrm{v}}$, one might be led to conclude that the VA parameters should simply be chosen as large as possible to maximise the provision of damping. To understand why this reasoning is erroneous, the response of the decoupled GFM controller is simulated for two grid disturbances: a $10°$ phase jump and a $25\,\%$ voltage dip. For the voltage dip, an ac-voltage controller (AVC) with a droop has been activated, which changes the reactive-power reference. To underline the differences, the parameter sets with the largest difference in $Z_{\mathrm{v}}$ are used: case 1, which is based on the lower gain limit ($L_{\mathrm{v}} = 0.676\,\mathrm{pu}$, $R_{\mathrm{v}} = 0.596\,\mathrm{pu}$), and case 5 combining the low decay time constant and more relaxed gain limit in the harmonic frequency range ($L_{\mathrm{v}} = 0.345\,\mathrm{pu}$, $R_{\mathrm{v}} = 0.126\,\mathrm{pu}$).

The simulation results are shown in Fig. 11 for the phase jump and in Fig. 12 for the voltage dip. Since the outer loops and their parameters are the same in both cases and only the VA parameters are changed, the results from both simulated disturbances demonstrate how the VA parameters impact the dynamic behaviour of the converter. The impact of the VA is in particular visible during the first couple of cycles after the disturbance, before the outer control loops have had time to react to the disturbance. In both cases, the parameter set based on case 5 shows a dynamic response with a higher current peak and a larger dc component, visible as a $50\,\mathrm{Hz}$ oscillation in active and reactive power.

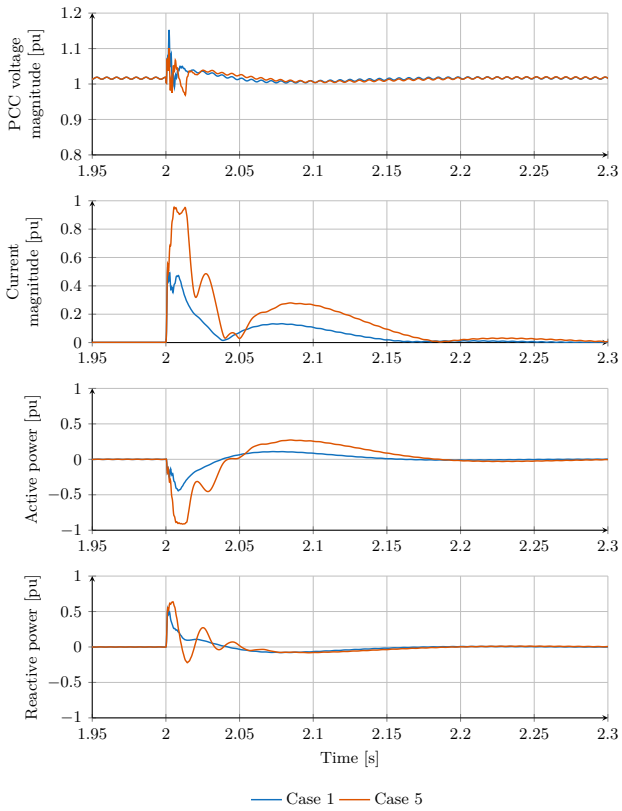


Fig. 11: Simulated response to a 10° phase jump at the grid's Thévenin voltage for the decoupled GFM controller with two different VA tunings.

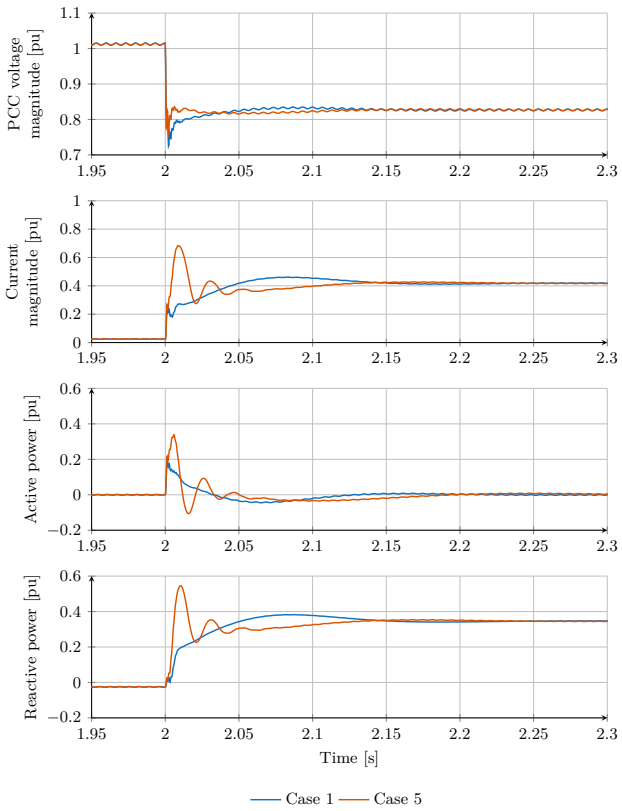


Fig. 12: Simulated response to a 25 % voltage dip at the grid's Thévenin voltage for the decoupled GFM controller with two different VA tunings.

As explained above, the dc component should be kept as small as possible. But this can not be generalised to assume that the converter's reaction to a grid disturbance should be as small as possible, i.e. that $Z_{\mathrm{v}}$ should be chosen to be big: the larger the VI, the larger the electrical distance between PCC and the converter's internal voltage source. As a consequence, the grid support and contribution to grid strength from the converter reduces as the impedance increases. Put in simple terms, VA parameters that are too large let the converter become a passive bystander – it does not negatively contribute to any control interactions, but it does not positively contribute to the stability of the grid during disturbances either.

Based on this, it could be assumed that the VA parameters should instead be selected to be as small as possible. But this would mean that even small disturbances in the grid would cause the converter's current or energy limiters[4] to saturate, and that the converter's linear control range would be very limited. It is therefore necessary to find a compromise between the advantages of large and small VA parameters. This compromise needs to take the conditions at the PCC, the system operator's requirements and the constraints of the converter system in question into account. Nevertheless, the tuning method presented above is an effective way to establish minimum values for the VA parameters that fulfil given performance requirements.

[4]As the energy stored in the capacitor on the converter's dc side is very limited in most applications, many converters are equipped with an energy limiter that prevents the dc voltage from varying too much [38].

## VI. Conclusions

This paper has demonstrated the frequency response that is expected of a GFM controller based on the analysis of a voltage source behind an impedance. Due to the possibility offered by the decoupled controller to freely select the VA parameters, a tuning method was required to determine these parameters according to the desired frequency response. The method proposed in this paper uses gain limits for the input admittance at selected frequencies. This approach is extended with the option for selecting a decay time constant of the dominant resonance in the VA. While the proposed tuning method cannot capture all aspects that can have an impact on the selection of the VA parameters, it provides an improvement of the methods available in the literature by offering an effective way for basing the tuning of the virtual resistance and inductance on the impact they have on the converter's frequency behaviour.

## References

[1] International Energy Agency, "Net Zero by 2050 - A Roadmap for the Global Energy Sector," Paris, France, Oct. 2021.

[2] B. K. Bose, "Global Energy Scenario and Impact of Power Electronics in 21st Century," *IEEE Transactions on Industrial Electronics*, vol. 60, no. 7, pp. 2638–2651, Jul. 2013, ISSN: 1557-9948.

[3] ENTSO-E, "High Penetration of Power Electronic Interfaced Power Sources and the Potential Contribution of Grid Forming Converters," 2020.

[4] J. Matevosyan, B. Badrzadeh, T. Prevost, *et al.*, "Grid-Forming Inverters: Are They the Key for High Renewable Penetration?" *IEEE Power and Energy Magazine*, vol. 17, no. 6, pp. 89–98, Nov. 2019, ISSN: 1558-4216.

[5] P. Rodriguez, I. Candela, C. Citro, J. Rocabert, and A. Luna, "Control of grid-connected power converters based on a virtual admittance control loop," in *2013 15th European Conference on Power Electronics and Applications (EPE)*, Sep. 2013, pp. 1–10.

[6] A. Narula, M. Bongiorno, and M. Beza, "Comparison of Grid-Forming Converter Control Strategies," in *2021 IEEE Energy Conversion Congress and Exposition (ECCE)*, Oct. 2021, pp. 361–368.

[7] J. D. V. Leon, A. Tarraso, J. I. Candela, J. Rocabert, and P. Rodriguez, "Grid-Forming Controller Based on Virtual Admittance for Power Converters Working in Weak Grids," *IEEE Journal of Emerging and Selected Topics in Industrial Electronics*, vol. 4, no. 3, pp. 791–801, Jul. 2023, ISSN: 2687-9743.

[8] P. Imgart, "Beyond Virtual Synchronous Machine Control," Chalmers University of Technology, 2025, ISBN: 978-91-8103-274-1.

[9] NERC, "White Paper: Grid Forming Functional Specifications for BPS-Connected Battery Energy Storage Systems," Sep. 2023.

[10] J. He, Y. W. Li, J. M. Guerrero, F. Blaabjerg, and J. C. Vasquez, "An Islanding Microgrid Power Sharing Approach Using Enhanced Virtual Impedance Control Scheme," *IEEE Transactions on Power Electronics*, vol. 28, no. 11, pp. 5272–5282, Nov. 2013, ISSN: 1941-0107.

[11] J. He, Y. W. Li, and F. Blaabjerg, "An Enhanced Islanding Microgrid Reactive Power, Imbalance Power, and Harmonic Power Sharing Scheme," *IEEE Transactions on Power Electronics*, vol. 30, no. 6, pp. 3389–3401, Jun. 2015, ISSN: 1941-0107.

[12] C. A. Macana and H. R. Pota, "Adaptive synchronous reference frame virtual impedance controller for accurate power sharing in islanded ac-microgrids: A faster alternative to the conventional droop control," in *2017 IEEE Energy Conversion Congress and Exposition (ECCE)*, Oct. 2017, pp. 3728–3735.

[13] R. An, Z. Liu, and J. Liu, "Successive-Approximation-Based Virtual Impedance Tuning Method for Accurate Reactive Power Sharing in Islanded Microgrids," *IEEE Transactions on Power Electronics*, vol. 36, no. 1, pp. 87–102, Jan. 2021, ISSN: 1941-0107.

[14] M. Keddar, M. L. Doumbia, K. Belmokhtar, and M. D. Krachai, "Experimental Validation of an Accurate Reactive Power-Sharing Approach Based on Adaptive Virtual Impedance and Consensus Control," in *2021 12th International Renewable Energy Congress (IREC)*, Oct. 2021, pp. 1–6.

[15] J. Zhang, Y. Jia, Z. Li, X. Ye, C. Yang, and D. Jiang, "Adaptive Virtual Impedance Control Strategy for Multiple Grid-forming Converters in Islanded Microgrid," in *2023 2nd Asia Power and Electrical Technology Conference (APET)*, Dec. 2023, pp. 599–604.

[16] C. Fan, X. Qin, L. Qi, H. Liu, B. Ding, and Z. Meng, "The Function Mechanism of Virtual Impedance in Grid-forming Droop Control and An Adaptive Parameter Tuning Method for Virtual Impedance Based on Network Equivalent Identification," in *2024 IEEE 2nd International Conference on Power Science and Technology (ICPST)*, May 2024, pp. 2171–2176.

[17] F. Salha, F. Colas, and X. Guillaud, "Virtual resistance principle for the overcurrent protection of PWM voltage source inverter," in *2010 IEEE PES Innovative Smart Grid Technologies Conference Europe (ISGT Europe)*, Oct. 2010, pp. 1–6.

[18] J. He and Y. W. Li, "Analysis, Design, and Implementation of Virtual Impedance for Power Electronics Interfaced Distributed Generation," *IEEE Transactions on Industry Applications*, vol. 47, no. 6, pp. 2525–2538, Nov. 2011, ISSN: 0093-9994.

[19] A. D. Paquette and D. M. Divan, "Virtual Impedance Current Limiting for Inverters in Microgrids With Synchronous Generators," *IEEE Transactions on Industry Applications*, vol. 51, no. 2, pp. 1630–1638, Mar. 2015, ISSN: 1939-9367.

[20] T. Qoria, F. Gruson, F. Colas, G. Denis, T. Prevost, and X. Guillaud, "Critical Clearing Time Determination and Enhancement of Grid-Forming Converters Embedding Virtual Impedance as Current Limitation Algorithm," *IEEE Journal of Emerging and Selected Topics in Power Electronics*, vol. 8, no. 2, pp. 1050–1061, Jun. 2020, ISSN: 2168-6777, 2168-6785.

[21] B. Wang, R. Burgos, and B. Wen, "Grid-Forming Inverter Control Strategy with Improved Fault Ride Through Capability," in *2022 IEEE Energy Conversion Congress and Exposition (ECCE)*, Oct. 2022, pp. 1–8.

[22] A. Bolzoni, G. M. Foglia, L. Frosio, M. F. Iacchetti, and R. Perini, "Impact of Line and Control Parameters on Droop Stability in Inverters for Distributed Generation," *IEEE Transactions on Smart Grid*, vol. 9, no. 6, pp. 6656–6665, Nov. 2018, ISSN: 1949-3061.

[23] A. Rodríguez-Cabero, J. Roldán-Pérez, and M. Prodanovic, "Virtual Impedance Design Considerations for Virtual Synchronous Machines in Weak Grids," *IEEE Journal of Emerging and Selected Topics in Power Electronics*, vol. 8, no. 2, pp. 1477–1489, Jun. 2020, ISSN: 2168-6785.

[24] D. Moutevelis, F. Göthner, J. Roldán-Pérez, and M. Prodanović, "Quasi-Stationary Implementation of Virtual Admittance Controller for Voltage Support from Distributed Generation," in *2022 IEEE PES Innovative Smart Grid Technologies Conference Europe (ISGT-Europe)*, Oct. 2022, pp. 1–5.

[25] X. Zhang, Y. Li, Y. Wen, J. Shen, C. Li, and S. Xiao, "Reactive Power Distribution of Mesh Parallel Distributed Generations Based on Virtual Impedance," in *2022 4th International Conference on Smart Power & Internet Energy Systems (SPIES)*, Dec. 2022, pp. 1254–1259.

[26] Z. Li, L. Liang, R. Yang, and X. Cai, "The Virtual Admittance Control of Sending End Converter for Offshore Wind Farm Integration," in *2023 IEEE 14th International Symposium on Power Electronics for Distributed Generation Systems (PEDG)*, Jun. 2023, pp. 133–136.

[27] O. Oboreh-Snapps, K. J. P. Veeramraju, A. Fernandes, *et al.*, "Small Signal Stability Analysis of Virtual Impedance Control in Islanded Microgrid," in *2023 IEEE Energy Conversion Congress and Exposition (ECCE)*, Oct. 2023, pp. 1005–1011.

[28] W. Zhang, J. Cui, Y. Zhao, and H. Yin, "Parameters Tuning of Flexible Drooped Synchronous Power Controller Based on Small Signal Modeling and Sensitivity Analysis," in *2023 IEEE 18th Conference on Industrial Electronics and Applications (ICIEA)*, Aug. 2023, pp. 886–891.

[29] E. Fedele, N. Campagna, G. Bossi, R. Rizzo, R. Miceli, and A. Damiano, "Stability Analysis of DFIG with Virtual-Admittance-Based Grid-Forming Control under Different Grid Strenghts," in *2024 6th Global Power, Energy and Communication Conference (GPECOM)*, Jun. 2024, pp. 399–404.

[30] K. Kamalinejad, A. Narula, M. Bongiorno, M. Beza, and J. R. Svensson, "Impact of Control Parameters on Angular Stability of Grid-Forming Converters Using Virtual-Admittance Based Control," in *2025 Energy Conversion Congress & Expo Europe (ECCE Europe)*, Sep. 2025, pp. 1–6.

[31] M. G. Taul, X. Wang, P. Davari, and F. Blaabjerg, "Current Limiting Control With Enhanced Dynamics of Grid-Forming

Converters During Fault Conditions," *IEEE Journal of Emerging and Selected Topics in Power Electronics*, vol. 8, no. 2, pp. 1062–1073, Jun. 2020, ISSN: 2168-6777, 2168-6785.

[32] L. Guo, S. Zhang, X. Li, Y. W. Li, C. Wang, and Y. Feng, "Stability Analysis and Damping Enhancement Based on Frequency-Dependent Virtual Impedance for DC Microgrids," *IEEE Journal of Emerging and Selected Topics in Power Electronics*, vol. 5, no. 1, pp. 338–350, Mar. 2017, ISSN: 2168-6785.

[33] Y. Zhao, W. Zhang, W. Wang, and Z. Pan, "Grid Forming Control with Inertial and Virtual Admittance Characteristics for Grid-tied Converters," in *2020 39th Chinese Control Conference (CCC)*, Jul. 2020, pp. 6164–6189.

[34] P. Imgart. "FreBaVAT - Frequency-Based Virtual-Admittance Tuning Script for Grid-Forming Converters." (Aug. 27, 2025), [Online]. Available: https://doi.org/10.5281/zenodo.16967617 (visited on 08/27/2025).

[35] L. Harnefors, M. Bongiorno, and S. Lundberg, "Input-Admittance Calculation and Shaping for Controlled Voltage-Source Converters," *IEEE Transactions on Industrial Electronics*, vol. 54, no. 6, pp. 3323–3334, Dec. 2007, ISSN: 1557-9948.

[36] Verband der Elektrotechnik Elektronik Informationstechnik e. V., *Technical requirements for grid connection of high voltage direct current systems and direct current-connected power park modules (VDE-AR-N 4131 TAR HVDC)*, Mar. 2019.

[37] L. Lu, O. Saborío-Romano, and N. A. Cutululis, "Torsional oscillation damping in wind turbines with virtual synchronous machine-based frequency response," *Wind Energy*, vol. 25, no. 7, pp. 1157–1172, 2022, ISSN: 1099-1824.

[38] J. Girona-Badia, "Grid-forming strategies for Renewable Energy Sources," Ph.D. dissertation, Universitat Politècnica de Catalunya, Barcelona, Spain, 2025.